The Institute of Space and Astronautical Science
Report SP No. 17 March 2003

A Thermochemical Nonequilibrium Flow around a Super Orbital Reentry Capsule with Ablation

By

Ryouji DOIHARA*, and Michio NISHIDA†

(1 February 2003)

Abstract: The aerodynamic heating to the super orbital reentry capsule of MUSES-C with ablation was numerically studied by using thermochemical nonequilibrium full viscous shock layer (VSL) equations. An 11 air-species model was used for non-ablating boundary conditions, and six carbonic species were added for ablating boundary conditions. With a three-temperature model, thermal nonequilibrium effect was taken into account. The convective and radiative heat fluxes to the wall were examined for both fully catalytic wall (FCW) condition and non-catalytic wall (NCW) condition at various altitudes for the capsule reentry trajectory path. The results of the ablation analysis at the altitude of 64 km showed that the stagnation heat fluxes with and without ablation are almost equal below the wall temperature of 3,000 K, whereas at the wall temperatures over 3,000 K, the stagnation heat flux is rapidly decreased with an increase in wall temperature due to significant sublimation.

1. INTRODUCTION

In the MUSES-C project the capsule is to enter into the earth's atmosphere directly from the hyperbolic earth-return trajectory. Therefore, the atmospheric entry speed of the capsule is over 12 km/s, so that a very strong shock wave is generated around the capsule, whereby the shock layer gas is much more highly heated than the case of a normal earth orbital reentry. Hence, it is predicted that radiative heat flux will be stronger in the super orbital reentry than in the earth orbital reentry. To make the effective design of the thermal protection system within the tightly limited weight, it is important to make more accurate estimation of aerodynamic heating and to reveal the degree of the contribution of the radiative heat flux.

A strong shock wave causes molecules of atmosphere to be dissociated and ionized, and consequently the shock layer gas will consist of molecules, atoms, ions and electrons. Density of air is quite low at high altitudes where characteristic times of chemical reactions and energy exchange will be of comparable order with the characteristic time of the flow or more.

* Department of Aeronautics and Astronautics, Kyushu University, Fukuoka 812-8581, JAPAN.
Present Address: Fluid Flow Division, Metrology Institute of Japan, National Institute of Advanced Industrial Science and Technology, Tsukuba 305-8563, JAPAN.
† Department of Aeronautics and Astronautics, Kyushu University, Fukuoka 812-8581, JAPAN.

Therefore, this flow field will be in thermochemical nonequilibrium. Under these conditions, translational, rotational, vibrational, electron and electronic temperatures are not essentially equal. Therefore, in order to analyze such a reentry flow field, thermochemical nonequilibrium cannot be avoided.

In this study the numerical analysis of the shock layer flow over the super orbital reentry capsule has been performed by using the thermochemical nonequilibrium viscous shock layer (VSL) equations. The VSL equations have been often used in order to analyze the nonequilibrium flow over a hypersonic body (Sakamura & Nishida 1991, Gupta 1996, Suzuki et al. 1996, Doihara & Nishida 2002). Of these, Suzuki et al. (1996) is cited as the work treating a super-orbital reentry. In their work, the flowfield over the MUSES-C capsule was analyzed using a two-temperature model consisting translational-rotational and vibrational-electron temperatures, and aerodynamic heating to the capsule for both FCW and NCW were discussed. In case of the super orbital reentry, radiative heat flux on the wall cannot be neglected. Intensity of radiation is strongly dependent on vibrational, electron and electronic temperatures, so that the thermal nonequilibrium should be calculated more accurately. The MUSES-C capsule will have a heat shield made of C/C composite material. The carbonic species will be ablated from the surface of the heat shield and may influence radiative heat flux. For this reason, a three-temperature model, in which translational-rotational, vibrational and electron-electronic temperatures are treated as different from each other, will be an adequate temperature model. To consider the effect of ablating species, 19 reactions of 6 carbonic species are added to the 11 air species model.

The present paper is concerned with the numerical analysis of the flow field over the super-orbital reentry capsule with ablation. The analysis uses a three temperature model for the reason mentioned above and nonequilibrium air chemistry is represented by using an 11 air species model and 6 carbonic species model. Furthermore radiative heat flux to the wall is estimated using SPRADIAN which is the computational code for estimating spectral intensity and radiative heat flux developed by Fujita & Abe (1997).

2. METHOD OF ANALYSIS

2.1 Governing Equations

The governing equations are the full viscous shock layer (FVSL) equations formulated for a multicomponent gas flow in thermochemical nonequilibrium. The VSL equations are obtained from the steady-state Navier-Stokes equations by retaining terms up to the second order in the Reynolds number parameter ϵ defined by $\epsilon = \sqrt{\mu_\infty/\rho_\infty U_\infty R_n}$ where μ_∞ is the viscosity at the free stream temperature, ρ_∞ the free stream density, U_∞ the free stream speed and R_n the nose radius of a body. These equations are written for an axisymmetric body-intrinsic coordinate system (s, y) as shown in Fig. 1. In the present study, the value of ϵ^3 is in the order of 10^{-2} to 10^{-4}, so that the VSL analysis is expected to provide sufficiently accurate solutions. In the full viscous shock layer (FVSL) analysis, the second order y-momentum equation is used.

The configuration of the reentry capsule is given by a hyperboloid with 20 cm in the nose radius and 45 deg in the semi-apex angle. (Fig. 1).

The following assumptions are introduced:

1) Rotational temperature of molecules is fully equilibrated with translational temperature of heavy particle.
2) Translational-rotational temperatures of all the species are equal.
3) Vibrational temperatures of all the molecular species are equal.

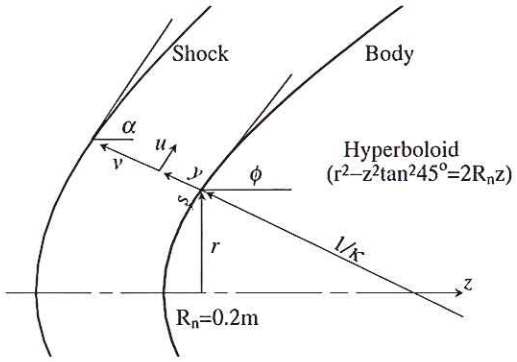

Fig. 1: Coordinate system.

4) Electronic temperatures of N, N^+, O, O^+, O_2 are equal and fully equilibrated with electron temperature.
5) Emission and absorption of radiation are not considered in the VSL calculation. Radiative heat flux is estimated from the results of the VSL analysis.

The present governing equations are composed of tangential momentum, normal momentum, translational-rotational energy, vibrational energy, electron-electronic energy and species conservation equations. They are written in fashion similar to Miner & Lewis (1975).

2.2 Transport properties

For the 11-species model, the transport properties are evaluated by extending Yos' formula, which is based on the first Chapman-Enskog approximation, to the multi-temperature gas mixture (Gupta et al. 1990). For ablation analysis, the viscosity and thermal conductivity for a mixture of gas have been computed using the Wilke's semi-empirical formula and Yos' formula. Viscosity of each species can be determined from the curve fit form of Blottner (1970) and the curve fit data for the species can be taken from Olynick et al. (1999). The diffusion coefficients of Curtiss & Hirschfelder (1949) are used. For ions, ambipolar diffusion is assumed.

2.3 Energy exchange

The energy transfer rate between translation and vibration is derived from the formula of the Landau-Teller model. The vibrational relaxation time is evaluated by an empirical formula of Millikan & White (1963) and the correction term of Park's collision limit (Park 1993). The translation-electron and rotation-electron energy transfer rates are taken from Lee (1985), and Lazdinis & Petrie (1974), respectively. In the energy exchange between vibrational and electron modes, only the vibrational energy of nitrogen is considered because the nitrogen-electron coupling is much stronger than others. The relaxation time of this exchange is taken from Lee (1992). The average vibrational energy removed by dissociation is assumed to be 50 % of dissociation energy.

2.4 Air chemistry

In case of the super orbital reentry, the temperature behind a shock exceeds 50,000 K. Molecules are fully excited at vibrational energy levels. At the same time these molecules dissociate into atoms and ionize into ions, so that we use an 11 species air (76.5 % N_2 + 23.5 % O_2 in the

freestream) model consisting of $N_2, O_2, NO, N, O, NO^+, O^+, N^+, N_2^+, O_2^+$ and e^-. We consider reactions of these 11 species given in Table 1. The chemical reaction rate model is the Park model (Park 1993) that uses effective temperature extended to a three temperature model. Reaction rates are assumed to be a function of controlling temperatures T_f and T_b depending on the type of reaction, and they are given by the following expressions:

$$k_{f,r}(T_{f,r}) = C_r T_{f,r}^{s_r} \exp(-\theta_r / T_{f,r}) \tag{1}$$

$$k_{b,r}(T_{b,r}) = k_{f,r}(T_{b,r}) / K_r^{eq}(T_{b,r}) \tag{2}$$

where $K_r^{eq}(T_{b,r}$ is the equilibrium constant. The controlling temperatures are shown in Table 1. The values of C_r, s_r and θ_r can be obtained from Park (1993).

For the ablation analysis, the 19 chemical reactions of 6 carbon-containing species are added to the 11 air species. The reaction rates of the 19 reactions are taken from Blottner (1970) and shown in Table 2.

Table 1: Chemical reactions of 11 air species.

r	Reactants		Products	T_f	T_b
1	$N_2 + M_1^a$	$\rightleftarrows$	$N + N + M_1$	$\sqrt{T \cdot T_{vib}}$	T
2	$N_2 + M_2^b$	$\rightleftarrows$	$N + N + M_2$	$\sqrt{T \cdot T_{vib}}$	T
3	$N_2 + e^-$	$\rightleftarrows$	$N + N + e^-$	$\sqrt{T_e \cdot T_{vib}}$	$\sqrt{T \cdot T_e}$
4	$O_2 + M_1$	$\rightleftarrows$	$O + O + M_1$	$\sqrt{T \cdot T_{vib}}$	T
5	$O_2 + M_2$	$\rightleftarrows$	$O + O + M_2$	$\sqrt{T \cdot T_{vib}}$	T
6	$NO + M_3^c$	$\rightleftarrows$	$N + O + M_3$	$\sqrt{T \cdot T_{vib}}$	T
7	$NO + M_4^d$	$\rightleftarrows$	$N + O + M_4$	$\sqrt{T \cdot T_{vib}}$	T
8	$N_2 + O$	$\rightleftarrows$	$NO + N$	T	T
9	$NO + O$	$\rightleftarrows$	$N + O_2$	T	T
10	$N + O$	$\rightleftarrows$	$NO^+ + e^-$	T	T
11	$N + N$	$\rightleftarrows$	$N_2^+ + e^-$	T	T
12	$O + O$	$\rightleftarrows$	$O_2^+ + e^-$	T	T
13	$NO^+ + O$	$\rightleftarrows$	$N^+ + O_2$	T	T
14	$O_2^+ + N$	$\rightleftarrows$	$N^+ + O_2$	T	T
15	$NO + O^+$	$\rightleftarrows$	$N^+ + O_2$	T	T
16	$O_2^+ + N_2$	$\rightleftarrows$	$N_2^+ + O_2$	T	T
17	$O_2^+ + O$	$\rightleftarrows$	$O^+ + O_2$	T	T
18	$NO^+ + N$	$\rightleftarrows$	$O^+ + N_2$	T	T
19	$NO^+ + O_2$	$\rightleftarrows$	$O_2^+ + NO$	T	T
20	$NO^+ + O$	$\rightleftarrows$	$O_2^+ + N$	T	T
21	$O^+ + N_2$	$\rightleftarrows$	$N_2^+ + O$	T	T
22	$NO^+ + N$	$\rightleftarrows$	$N_2^+ + O$	T	T
23	$N + e^-$	$\rightleftarrows$	$N^+ + e^- + e^-$	T_e	T_e
24	$O + e^-$	$\rightleftarrows$	$O^+ + e^- + e^-$	T_e	T_e

[a] $M_1 = N_2, O_2, NO, N_2^+, O_2^+, NO^+$
[b] $M_2 = N, O, N^+, O^+$
[c] $M_3 = N_2, O_2, N_2^+, O_2^+$
[d] $M_4 = NO, N, O, NO^+, N^+, O^+$

2.5 Solution procedure

In the VSL analysis, the equations of tangential-momentum, translational-rotational energy, vibrational energy, electron-electronic energy and species conservation are written in the same

Table 2: Chemical reactions of 6 carbon-containing species.

r	Reactants		Products
1	$CO_2 + M_1$	$\rightleftharpoons$	$CO + O + M_1$
2	$CO + M_2$	$\rightleftharpoons$	$C + O + M_2$
3	$C_2 + M_3$	$\rightleftharpoons$	$C + C + M_3$
4	$C_3 + M_4$	$\rightleftharpoons$	$C_2 + C + M_4$
5	$CN + M_5$	$\rightleftharpoons$	$C + N + M_5$
6	$N_2 + C$	$\rightleftharpoons$	$CN + N$
7	$CO + N$	$\rightleftharpoons$	$CN + O$
8	$CO_2 + N$	$\rightleftharpoons$	$CN + O_2$
9	$N_2 + CO$	$\rightleftharpoons$	$CN + NO$
10	$CO + NO$	$\rightleftharpoons$	$CO_2 + N$
11	$CO_2 + O$	$\rightleftharpoons$	$CO + O_2$
12	$2CO$	$\rightleftharpoons$	$CO_2 + C$
13	$CO + O$	$\rightleftharpoons$	$O_2 + C$
14	$CO + N$	$\rightleftharpoons$	$C + NO$
15	$CN + O$	$\rightleftharpoons$	$C + NO$
16	$2CO$	$\rightleftharpoons$	$C_2 + O_2$
17	$CO + C$	$\rightleftharpoons$	$C_2 + O$
18	$C_2 + CO$	$\rightleftharpoons$	$C_3 + O$
19	$C_3 + C$	$\rightleftharpoons$	$2C_2$

$M_j = \sum_i Z_{ki} X_i$

Z_{ki} Third body Efficiencies relative to Argon

$i=$	1	2	3	4	5	6	7	8	9	10	11	12
	O_2	N_2	O	N	NO	NO^+	CO	CO_2	C	C_2	C_3	CN
M_1	2	2	2	2	2	0	2	5	1	1	1	1
M_2	1	1	1	1	1	0	1	1	1	1	1	1
M_3	1	1	1	1	1	0	1	1	1	1	1	1
M_4	1	1	1	1	1	0	1	1	1	1	1	1
M_5	1	1	1	1	1	0	1	1	1	1	1	1

standard parabolic form as Miner & Lewis (1975). These equations are rewritten in a tridiagonal matrix by using a second order finite difference method. The tridiagonal matrix is easily solved using the Thomas algorithm. However in this study, numerical instabilities occur in overall iteration of these equations because of the usage of a three temperature model. To avoid this, a relaxation term $(W^{k+1} - W^k)/\Delta$ is added to the standard parabolic form:

$$\frac{W^{k+1} - W^k}{\Delta} = \frac{\partial^2 W^{k+1}}{\partial \eta^2} + A_1 \frac{\partial W^{k+1}}{\partial \eta} + A_2 W^{k+1} + A_3 + A_4 \frac{\partial W^{k+1}}{\partial \xi}, \tag{3}$$

where k is the iteration number, Δ is the relaxation parameter, W represents the normalized physical value of $u, T, T_{\rm vib}, T_{\rm e}$ and C_i. If the number of iteration is sufficient for convergence of $W^{k+1} \to W^k$, this equation becomes the same as the standard parabolic equation. Using this method, the equations can be solved asymptotically. First, the VSL equations on the stagnation streamline are solved. Next, the downstream portion is calculated by a space marching method where an initial shock profile is assumed to be parallel to a body surface. Then, shock layer

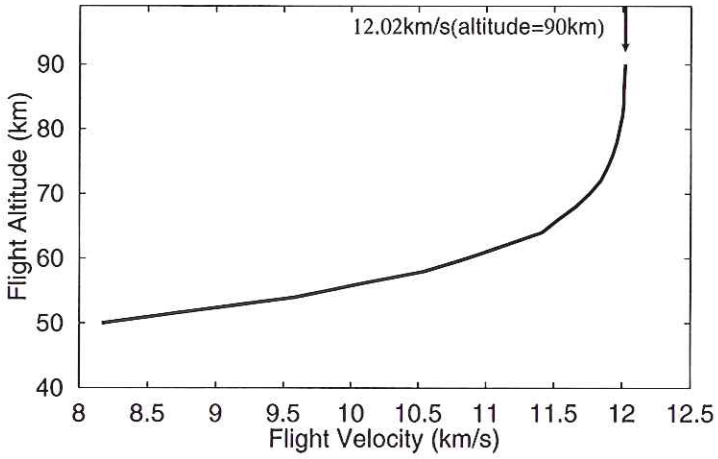

Fig. 2: Reentry trajectory of MUSES-C.

properties are determined and the shock profile is refined. For the new shock profile, the VSL equations are newly solved iteratively until the shock layer properties do not change. In the present calculation, 101 grid points are put between the body and shock in the direction normal to the body.

2.6 Boundary Conditions

At the wall, no-slip conditions ($u = v = 0$) are imposed. The species wall boundary conditions are determined by using either noncatalytic wall (NCW) condition $(\partial C_i/\partial y)_{\mathrm{w}} = 0$ or fully catalytic wall (FCW) condition $C_i = C_{i_\infty}$, where C_i is the mass concentration of species i. The wall temperature T_{w} is assumed to be constant at 2,500 K in the non-ablation analysis. The vibrational temperature on the wall is also assumed to be equal to the wall temperature. The boundary condition of the electron temperature is calculated by Eq.(10) in Nishida (1972) that is derived from the Langmuir probe theory. Boundary conditions immediately behind the shock are determined by shock jump conditions from free stream conditions on the reentry trajectory (Fig. 2). To consider low density gas effect, shock boundary conditions are determined by using shock slip conditions (Miner & Lewis 1975). Vibrational temperature and electron temperature are set to being equal to the freestream temperature.

For the ablation analysis, we consider the sublimation of C_3 and the oxidation by atomic oxygen as ablating boundary conditions. The oxidation by O_2 is not considered because the reaction probability is negligibly small in comparison with that by atomic oxygen. The O and CO mass fluxes due to oxidation are given as

$$J_{\mathrm{O,oxi}} = -\rho_{\mathrm{O}} K_{\mathrm{w,oxi}}, \quad J_{\mathrm{CO,oxi}} = \frac{M_{\mathrm{CO}}}{M_{\mathrm{O}}} \rho_{\mathrm{O}} K_{\mathrm{w,oxi}} \tag{4}$$

where

$$K_{\mathrm{w,oxi}} = \alpha \sqrt{\frac{RT_{\mathrm{w}}}{2\pi M_{\mathrm{O}}}} \tag{5}$$

and M_{CO} and M_O are, respectively, the molecular weights of CO and O. The reaction probability α is given as follows (Park 1976) :

$$\alpha = 0.63 \exp(-1160/T_w) \tag{6}$$

The sublimation of C and C_2 is not considered, since their equilibrium vapor pressure is much lower than that of C_3. The mass flux due to sublimation of C_3 is given by the Hertz-Knudsen-Langmuir relation (Blottner 1970):

$$J_{C_3,sub} = \frac{\alpha_{C_3} \cdot Max(0, P_{e,C_3} - P_{C_3})}{\sqrt{2\pi(R/M_{C_3})T_w}} \tag{7}$$

where P_{e,C_3} and P_{C_3} are equilibrium vapor pressure and partial pressure, respectively. The value of constants of α_{C_3} and P_{e,C_3} were given in Blottner (1970).

2.7 Radiation Calculation

The VSL analysis is not coupled with the calculation of radiative heat transfer. Radiation analysis is performed by SPRADIAN (Fujita & Abe 1997) in non coupled manner, using flow field on the stagnation stream line calculated by the VSL code. In the estimation of radiative heat flux, the spherical cap model (Fujita & Abe 1997) is used for the integration of the heat transfer equation.

3. RESULTS AND DISCUSSION

The non-ablation analysis revealed that the heat fluxes for FCW and NCW have the maximum of 8.7 MW/m^2 at the altitude of 56 km and 6.1 MW/m^2 at the altitude of 56 km, respectively. the radiative heat transfer becomes significant at the altitudes from 70 km to 55 km. At these altitudes, so called avalanche ionization phenomenon (Park 1990) leads to larger electron density and temperature, and as a result radiative heating becomes strong. The maximum radiative heating is approximately 0.9 MW/m^2 at the altitude of 62 km. The difference between the radiative heat fluxes for NCW and FCW cannot be seen. On the other hand,

Figures 3 and 4 illustrate the results of the ablation analysis, that is the distribution of the mole fractions on the stagnation streamline (H =64 km, T_w=2,500 K, 19 species model). In all the ablation analyses, the air species are assumed to be fully catalytic on the wall. It can be seen that the degree of ionization becomes fairly high and dominant species are N, O, N^+ and e^-. The mole concentration of the electron increases in the region from 0.5 to 0.3 which is attributed to the electron-impact ionization ($N + e^- \rightarrow N^+ + e^- + e^-$). The rate coefficient for this reaction is intrinsically large because of the high thermal speed of electrons. If electron temperature and density become over certain high values, this process occurs as a chain reaction. It is said that this phenomenon, called "Avalanche Ionization", is one of the characteristics of a super orbital flight velocity (Park 1990). At this wall temperature (T_w=2,500 K), the oxidation is significant. The mole fractions of CO and C are large in these carboncontaining species.

Figure 5 shows the mole fractions of carbonic species on the stagnation streamline in case of T_w = 3,200 K. It is seen that the mol fraction of C_3 is comparatively large in the vicinity of the wall, that means significant sublimation of C_3. In the region away from the wall, C_3 is

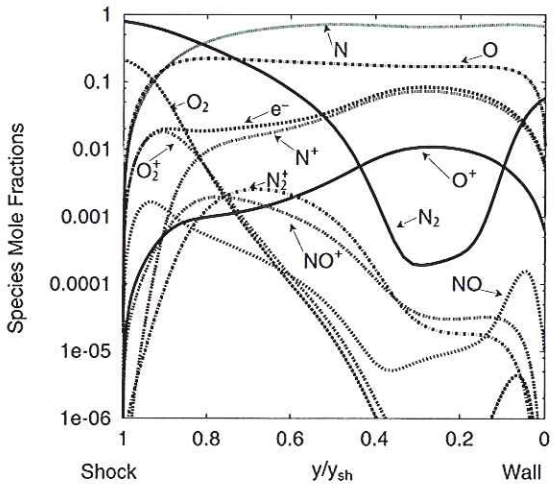

Fig. 3: Mole fractions of air species on the stagnation streamline (H = 64 km, T_w = 2,500 K).

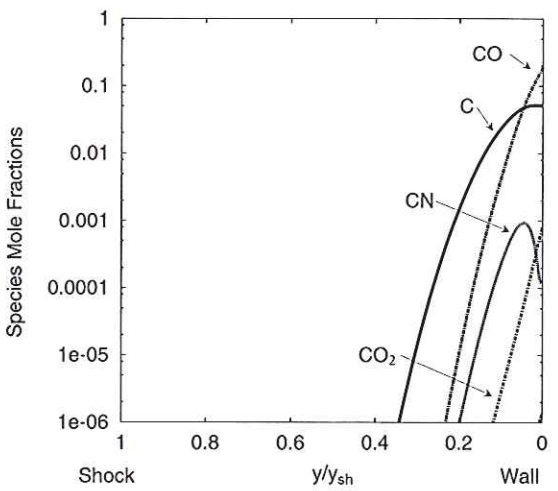

Fig. 4: Mole fractions of carbonic species on the stagnation stream line (H = 64 km, T_w = 2,500 K).

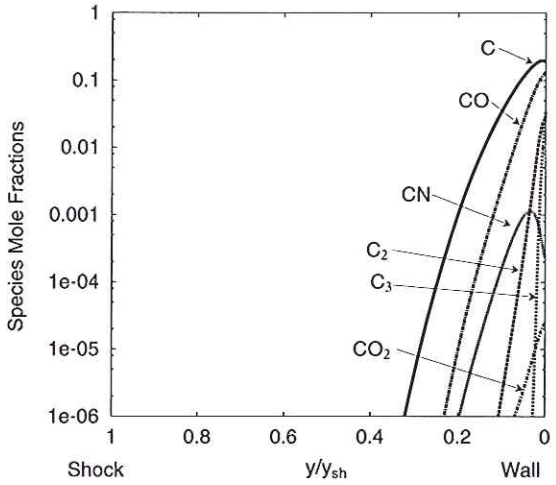

Fig. 5: Mole fractions of carbonic species on the stagnation stream line (H = 64 km, T_w = 3,200 K).

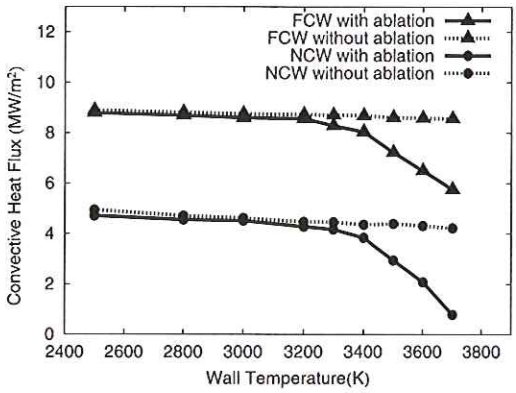

Fig. 6: Variations of stagnation heat flux vs wall temperature (H = 64 km).

rapidly dissociated into C_2 and C, and then these two species and air species recombined into CN and CO_2.

Figure 6 shows the variations of the stagnation heat flux with the wall temperature in the ablation analysis at the altitude of 64 km. At T_w= 2,500 K, the stagnation heat fluxes with and without ablation are almost equal. At the wall temperatures above 3,000 K, where the sublimation becomes significant, the stagnation heat flux with ablation is rapidly reduced.

Figure 7 illustrates radiation spectra with and without ablation that was calculated by SPRADIAN (Fujita & Abe 1997) on the stagnation point at the altitude of 64 km (T_w=3,200 K). The strong emission line spectra from N, N^+ and O are identified below 2,000 Å and over 7,000

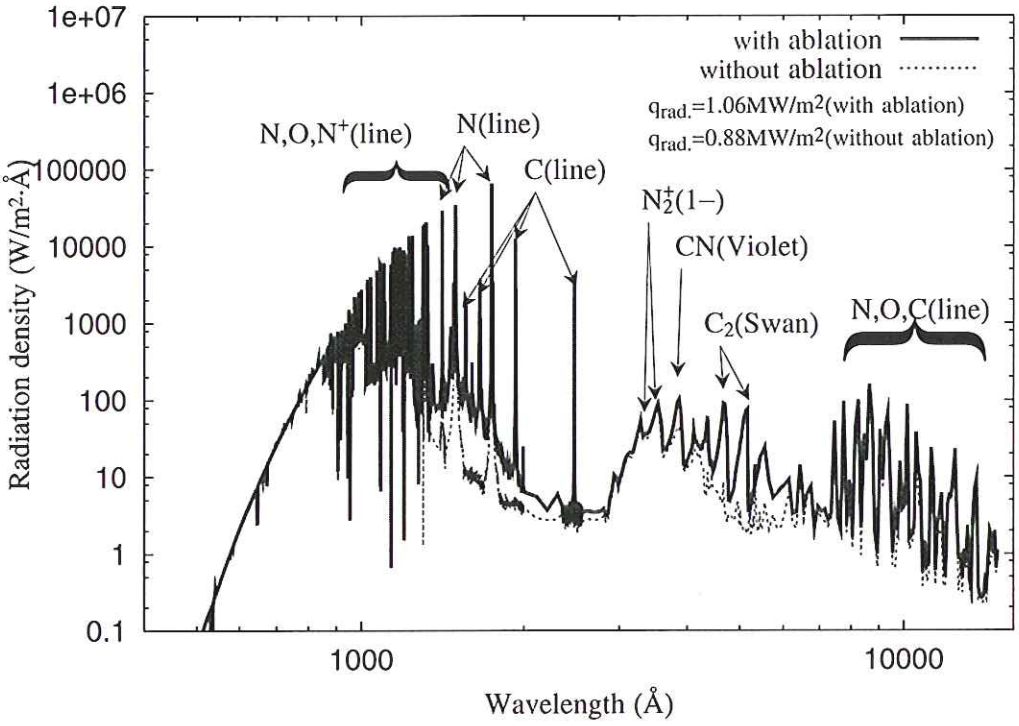

Fig. 7: Radiation density at the stagnation point with ablation (H = 64 km, T_w = 3,200 K).

Å. N_2^+(1-) band spectra are also observed in the range from 3,000 Å to 5,000 Å. The radiative heat flux without ablation is 0.86 MW/m^2. In the spectra with ablation, line spectra of C and band spectra of CN(Violet) and C_2(Swan) are observed. The radiative heat flux with ablation is 0.96 MW/m^2.

4. CONCLUDING REMARKS

Aerodynamic heating to the super orbital reentry capsule has been numerically analyzed by using the full viscous shock layer equations with a three temperature model and nonequilibrium air chemistry.

It has been found from the non-ablation analysis that the heat fluxes for FCW and NCW have the maximum of 8.7 MW/m^2 at the altitude of 56 km and 6.1 MW/m^2 at the altitude of 56 km, respectively. The radiative heat flux evaluated from the calculated flow properties has the maximum of 0.9 MW/m^2 at the altitude of 62 km for both NCW and FCW.

The ablation by the sublimation becomes significant at the wall temperature higher than 3,000 K and reduces the wall heat flux largely. On the other hand, when the wall temperature is low, the ablation occurs only by the oxidation, which leads to the fact that the wall heat flux is hardly reduced by the ablation due to oxidation. The ablation species slightly increase the radiative heat flux.

REFERENCES

Blottner, F.G., 1970, Prediction of electron density in the boundary layer on entry vehicles with ablation, NASA SP-252, pp. 219–240.

Curtiss, C.F., Hirschfelder, J.O., 1949, Transport properties of multi component gas mixture, J. Chem. Phys., Vol. 17, pp. 550–555.

Doihara, R., Nishida, M., 2002, Thermochemical nonequilibrium viscous shock layer studies of the orbital reentry experiment (OREX) vehicle, Shock Waves, Vol. 11, pp. 331–339.

Fujita, K., Abe, T., 1997, SPRADIAN, Structured package for radiation analysis: theory and application, ISAS Report 669.

Gupta, R.N., Yos, J.M., Thompson, R.A., Lee, K.P., 1990, A review of reaction rates and thermodynamic and transport properties for the 11-species air model for chemical and thermal nonequilibrium calculations to 30000K, NASA RP-1232.

Gupta, R.N., 1996, Viscous shock-layer study of thermochemical nonequilibrium, J. Thermophys. Heat Transfer, Vol. 10, pp. 257–266.

Lazdinis, S.S., Petrie, S.L., 1974, Free electron and Vibrational temperature nonequilibrium in high temperature nitrogen, Phys. Fluids, Vol. 17, pp. 1539–1546.

Lee, J.H., 1985, Basic governing equations for the flight regimes of aeroassisted orbital transfer vehicles, AIAA Progress in Astronautics and Aeronautics, Vol. 96, pp. 3–53.

Lee, J.H., 1992, Electron-impact vibrational relaxation in high-temperature nitrogen, AIAA Paper 92-0807.

Millikan, R.C., White, D.R., 1963, Systematics of vibrational relaxation, J. Chem. Phys., Vol. 139, pp. 34–43.

Miner, E.W., Lewis, C.H., 1975, Hypersonic ionizing air viscous shock-layer flows over nonanalytic blunt bodies, NASA CR-2550.

Nishida, M., 1972, Nonequilibrium viscous shock layer in a partially ionized gas, Phys. Fluids, Vol. 15, pp. 596–602.

Olynick, D., Chen, Y.K., Tauber, M.E., 1999, Aerothermodynamics of the stardust sample return capsule, J. Spacecraft & Rockets, Vol. 36, pp. 442–462.

Park, C., 1976, Effects of atomic oxygen on graphite ablation, AIAA journal, Vol. 14, pp. 1640–1642.

Park, C., 1990, Nonequilibrium hypersonic aerothermodynamics, (John Wiley & Sons, Inc. New York), p.167.

Park, C., 1993, Review of chemical-kinetic problems of future NASA missions, I: Earth entries, J. Thermophys. Heat Transfer, Vol. 7, pp. 385–398.

Sakamura, Y., Nishida, M., 1991, Numerical calculation of thermal and chemical nonequilibrium flows around a hypersonic reentry vehicle, Trans. Japan Soc. Aero. Space Sci., Vol. 34, pp. 27–45.

Suzuki, K., Kubota, H., Fujita, K., Abe, T., 1996, Numerical analysis of aerodynamic heating on MUSES-C reentry capsule, Proc. 20th International Symposium on Space Technology and Science, Gifu, Japan, ISTS 96-d-25.